Flow-Dependent Filtration of a Rigid-Rod Polymer

Robert P. Adamski

Shell Development Company, Houston, Texas

John L. Anderson*

Department of Chemical Engineering, Carnegie Mellon University, Pittsburgh, Pennsylvania 15213

Received October 11, 1990; Revised Manuscript Received February 7, 1991

ABSTRACT: Dilute solutions of poly(1,4-phenylene-2,6-benzobisthiazole) (PBT) in methanesulfonic acid were filtered through microporous mica membranes to study effects of solvent flow rate on the rejection of rodlike molecules. Two PBT polymers having mean lengths of 1180 and 1800 Å were used, and the pore diameter of the membranes was in the range 600–900 Å. The reflection coefficient for the polymer (σ), defined as the fraction of polymer rejected by the pores, decreased as the flow rate per pore (q) increased above $0.1(kT/\eta_s)$, where η_s is the solvent viscosity. The zero-flow limit of σ was about 0.8, a value that is consistent with a theory based on steric interactions between rodlike molecules and circular cylindrical pores. The dependence of σ on the dimensionless flow parameter $q\eta_s/kT$ for the rodlike PBT is quantitatively similar to that for linear polystyrene in a good solvent, even though the conformations of these two polymers are different and the solvent viscosity used for each polymer solution differs by a factor of 20.

Introduction

The filtration of flexible linear polymers through microporous membranes is flow-rate dependent.[1-4] Solvent flow into the entrance of the pores is strongly extensional, and at sufficiently large flow rates the polymer chains undergo a coil–stretch transformation[5,6] enabling a significant number of them to pass through pores having diameters that are *smaller* than the mean unperturbed dimension of the chain. Daoudi and Brochard[7] and de Gennes[8] developed a semiquantitative model (DBG model) for the deformation of a chain as it follows a streamline toward the pore entrance. Assuming affine deformation, i.e., the polymer chain deforms with the fluid at fixed segment density, they derived an expression for the critical flow rate per pore (q_{crit}) necessary to stretch and align a polymer molecule such that it will enter and pass through a pore that is smaller than the undeformed chain:

$$q_{crit} \sim kT/\eta_s \tag{1}$$

where η_s is the viscosity of the solvent and kT is the thermal energy. In this model the filtration of flexible chains is envisioned as a first-order transition, with essentially no passage of the polymer when $q < q_{crit}$ and total passage when $q > q_{crit}$. A most important prediction of the model is that q_{crit} is independent of the polymer's molecular weight or equivalently the mean dimension of the polymer chain.

Experiments with narrow molecular weight fractions of linear polystyrene ($10^5 <$ MW $< 10^7$) in dilute solutions have demonstrated flow-induced passage of flexible polymers when q was of order kT/η_s, even though the pores were a factor of 2 or 3 smaller than the hydrodynamic radius of the polymer.[2-4] However, there was not a sharp transition with increasing flow rate, as suggested by the DBG model, rather the fraction rejected (σ) was a steadily decreasing function of the solvent flow rate through each pore with the following asymptotic behavior:

$$s \to 0: \quad \sigma = 1 - 3.6s^{1.69} \tag{2a}$$

$$s \gtrsim 1: \quad \sigma \sim s^{-n} \quad (n \approx 1/2) \tag{2b}$$

where $s = q\eta_s/kT$. These experiments were consistent with the DBG model in that the dependence of σ on q was *independent* of *molecular weight* for linear polystyrene. One possible explanation for the lack of a sharp transition in σ with increasing flow rate is the considerable vorticity in the solvent velocity near the membrane surface; thus the point–sink model for the velocity field, assumed in the DBG theory, is not correct for membrane filtration. By accounting for the shear components of the velocity field, Keh[9] has derived eq 2b with $n = 1/2$.

A second limitation of the DBG model is that it does not consider the effect of chemical structure, e.g., chain branching or rigidity, on the filtration behavior of a polymer molecule. Experiments with star- and comb-branched polystyene have shown that chemical structure is important.[4] Highly branched polymers exhibit greater rejection than linear polymers at a given solvent flow rate. This result is consistent with the notion that branched polymers are more difficult to deform and hence less susceptible to coil–stretch transitions.

Since slender rods align in extensional flows when the extension rate exceeds the rotational diffusion coefficient,[10] we anticipate that a strong entrance flow into a pore during ultrafiltration will align rodlike polymers and force their passage even when the length of the rod is greater than the pore diameter. A semiquantitative theory for such alignment and flow-dependent passage of rigid rods was proposed by Auvray.[11] This model follows the original arguments leading to the DBG model for flexible chains and similarly predicts a strong-flow limit, $q \gtrsim kT/\eta_s$, above which essentially all the rods are aligned by the time they are convected to the pore entrance with the result $\sigma \to 0$. One difference between rigid-rod and flexible polymers, pointed out by Auvray, is that in the weak-flow limit, $q \ll kT/\eta_s$, $\sigma \approx 1$ for flexible polymers having a radius of gyration greater than the pore radius, whereas a significant number of rigid rods will pass ($\sigma < 1$) even when their length is comparable to the pore diameter.

In this paper we report data for the flow-dependent filtration of a rodlike polymer, poly(1,4-phenylene-2,6-benzobisthiazole) (PBT). The polymer solutions were very dilute and the membranes had a low area fraction of pores. The membranes were made by a track-etch process, which produces pores that are uniform in size and oriented

0024-9297/91/2224-3562$02.50/0

Table I
Properties[a] of the Two Samples of Poly(1,4-phenylene-2,6-benzobisthiazole) (PBT)

	PBT-A	PBT-S
stock soln, wt % in poly(phorphoric acid)	9.2%	3.0%
M_w/M_n	≈2	≈2
$[\eta]$, cm³/gm	1400	3000
L, Å	1180	1800
d, Å	7.0	7.0

[a] M_w and M_n are weight- and number-average molecular weights, $[\eta]$ is the intrinsic viscosity, L is the equivalent rod length of the chain (from eq 3), and d is the diameter of the rod. Values of M_w/M_n and $[\eta]$ were obtained from G. C. Berry and C. Spencer.[12]

perpendicular to the faces of the membrane. The uniformity of pore size is important because we can interpret the passage of polymer across the membrane in terms of events occurring at the level of a single pore.

Experiments

Two samples of poly(1,4-phenylene-2,6-benzobisthiazole), labeled PBT-A and PBT-S, were obtained as 9% and 3% by weight solutions in poly(phosphoric acid), respectively.[12] Physical properties of these samples are listed in Table I. The polydispersity (M_w/M_n) was about 2 for both samples. Rheological measurements indicate PBT is essentially a rigid rod.[13] The mean length of the polymer, L (Å), is determined from the measured low-shear intrinsic viscosity, $[\eta]$ (cm³/gm), by using the following formula:[13,14]

$$L = 21.1[\eta]^{5/9} \tag{3}$$

PBT is soluble in aprotic solvents, but small amounts of water cause aggregation of the molecules, most likely in a side-to-side arrangement rather than end to end.

Solutions of PBT in methanesulfonic acid (MSA) were made by diluting the poly(phosphoric acid) stock solution with MSA. The MSA was purified by multiple distillations to remove water and then stored under a dry nitrogen blanket before making the PBT solutions. All PBT solutions were made inside a glovebox in which a dry nitrogen atmosphere was maintained. We experimentally determined the viscosity of polymer-free MSA (η_s, centipoise) as a function of temperature (K) and obtained the following result:

$$\ln \eta_s = -7.360 + \frac{2921}{T} \tag{4}$$

The concentration of PBT in MSA was usually about 3×10^{-6} gm/cm³ and was determined by light absorption at 442 nm. Because of a high extinction coefficient, concentrations as low as 10^{-7} gm/cm³ could be detected. The very dilute concentration range for rigid rods is given by

$$\frac{\pi}{6} L^3 N_A \frac{C}{M} < 1 \tag{5}$$

where C is the mass concentration, M is the molecular weight, and N_A is Avogadro's number. For PBT, $M = 22L$ where L is in angstroms. For our two samples of PBT, this equation gives 5.0×10^{-5} and 2.1×10^{-5} gm/cm³, both of which are above the concentration of PBT used in our filtration experiments; therefore, we can safely assume that steric interactions between PBT molecules were negligible.

The membranes were made from thin sheets (≈7–8 μm) of muscovite mica by the track-etch process, which produces uniform, parallel pores having a 60° rhomboidal cross section.[15,16] The membrane area containing the pores (the "irradiated area") was 2 cm², located at the center of the mica disk, which was 5.5 cm in diameter. The pore radius (R) is defined as the radius of a circle having the same cross-sectional area as the pore. Characteristics of the five membranes used in these experiments are given in Table II. The pore radius was determined by measuring the pressure drop versus MSA flow rate in the absence of PBT and using Poiseuille's equation (see eq A8) with a modification for the rhomboidal shape of the pores.[4] At the highest porosities, there was some overlap of single pores to form doublets; an estimate of the fraction of pores that were singlets is given for each membrane in Table II. A discussion of the statistics of pore overlap and effects on our filtration experiments is presented in the Appendix.

Table II
Properties of Porous Mica Membranes[a]

membrane	$10^{-6}n$	l, μm	R, Å	$\bar{\phi}$, %	x_1
M23	5.92	7.84	470	2.0	0.96
M24	7.36	7.54	400	1.9	0.96
M25	23.6	7.12	320	3.8	0.92
M26	7.15	7.46	460	2.4	0.95
M27	21.9	7.58	440	6.6	0.87

[a] n is the number of tracks in the irradiated portion of the membrane; l is the membrane thickness, which equals the pore length for these membranes; R is the pore radius determined from the pressure–flow rate data and eq A8 of the Appendix; and $\bar{\phi} = n\pi R^2/A$ where A is the irradiated portion of the membrane (2 cm²). x_1 is the fraction (n_1/n) of tracks that were etched into singlets, as computed from (A3) with ϕ_0 given by (A11).

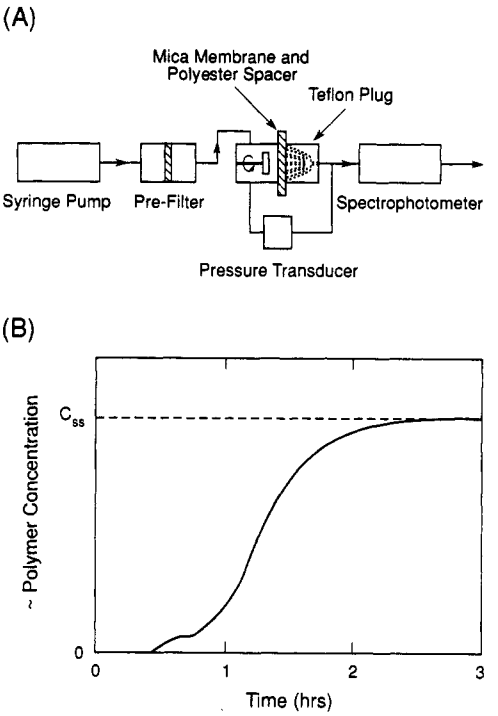

Figure 1. (A) Filtration apparatus. (B) Typical absorbance trace from flow-through spectrophotometer. PBT concentration was proportional to the absorbance at 442 nm.

The apparatus for performing the filtration experiments is shown schematically in Figure 1A. The prefilter was a mica membrane with pores 0.25 μm in radius. The volume of the high-pressure side of filtration cell was 16.5 cm³, while the low-pressure reservoir was a Teflon plug with small holes drilled through it. The total dead volume on the low-pressure side up to the spectrophotometer cell was slightly less than 1 cm³, and the spectrophotometer cell had a hold-up of less than 0.05 cm³. With a membrane placed in the filtration cell, filtered MSA without PBT

was loaded into the high-pressure side; this was accomplished inside a glovebox to reduce chances of contamination by water. The filtration cell was sealed by closing all sampling ports and then removed from the glovebox. Polymer-free, prefiltered MSA was then forced at different flow rates through the filtration membrane to determine its pore radius.

PBT was loaded into the high-pressure side of the filtration cell by first passing the solution through the prefilter and then flushing the high-pressure side of the filtration cell with this solution *without flow* through the membrane (another sampling valve connected to the high-pressure side was open). When the concentration of PBT reached the desired level ($C_H \approx 3 \times 10^{-6}$ gm/cm^3), the PBT prefilter was disconnected and the sampling valve was closed. The syringe pump was then turned on to force polymer-free, prefiltered MSA into the high-pressure side, which resulted in a constant flow rate across the membrane. The effluent from the low-pressure side of the filtration cell was directed through the spectrophotometer to determine the concentration of PBT and then into discrete sampling vials. A precise measure of the flow rate across the membrane was determined by weighing the sampling vials. At the end of one experiment, a sample of the high-pressure side solution was taken to remeasure C_H, the setting on the syringe pump was changed to increase or decrease the flow rate through the membrane, and another filtration experiment was started. Six or seven experiments were run consecutively in this manner with one membrane, without adding more PBT to the system. Less than 3 cm^3 of MSA flowed through the membrane in any experiment, and the PBT concentration in the high-pressure side (C_H) decreased 5% or less over the duration of an experiment. The ranges of membrane pressure drop and overall MSA flow rate were 0–0.2 bar and 0–0.5 cm^3/h, respectively.

A typical concentration trace of the ultrafiltrate as a function of time is shown in Figure 1b. At times greater than the residence time of the fluid in the low-pressure side of the filtration cell, the concentration of PBT reached an apparent steady value, C_{ss}. The reflection coefficient (σ) is defined as the fraction of polymer retained by the membrane; it is related to the mass transfer rate ($\dot{m}$) of PBT across the membrane by

$$\dot{m} = (1 - \sigma)C_H Q \tag{6}$$

where Q is the MSA flow rate and C_H is the PBT concentration in the high-pressure side of the filtration cell. The concentration of PBT (C^*) in the solution flowing through the membrane is related to the mass flux by

$$C^* = \dot{m}/Q \tag{7}$$

After enough time has elapsed to purge solvent from the dead volume in the low-pressure side, C_{ss} should equal C^*. Combining the above two relations gives

$$\sigma = 1 - \frac{C_{ss}}{C_H} \tag{8}$$

C_{ss} would be a true steady-state concentration if C_H were constant; however, because PBT-free solvent was injected by the syringe pump into the high-pressure side of the filtration cell, C_H decreased slightly with time ($\lesssim$5% over the experiment). To correct for these small changes, we used the arithmetic mean of C_H, determined from the measured high-pressure side concentration of PBT before and after the experiment. The error in σ arising from changes in C_H is expected to be ± 0.01 when $\sigma > 0.5$ and increases to ± 0.05 as σ approaches 0.

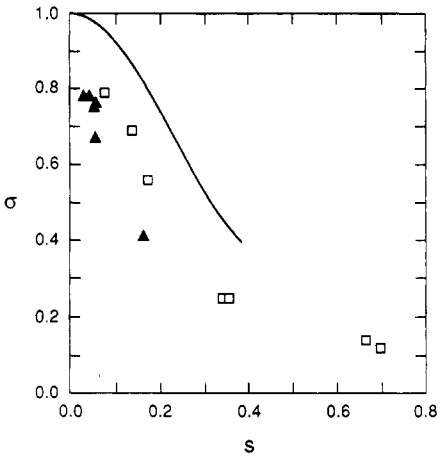

Figure 2. Reflection coefficient of PBT-A. $s = q\eta_s/kT$, where q is the MSA flow rate per pore and η_s is the MSA viscosity. The curve is eq 14, which represents data[4] for linear polystyrene in good solvents. Symbol/membrane: □/M26; ▲/M27.

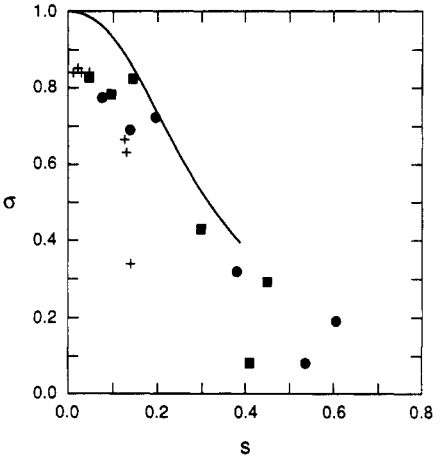

Figure 3. Reflection coefficient of PBT-S. $s = q\eta_s/kT$. The curve is eq 14, which represents data[4] for linear polystyrene in good solvents, given by eq 14. Symbol/membrane: ●/M23; ■/M24; +/M25.

The high-pressure side of the filtration cell was stirred by rotating a magnetic bar at 240 rpm. Previous studies with polystyrene filtration[4] indicate that this stirring rate is sufficient to render insignificant any boundary-layer effects at the membrane surface, thereby avoiding buildup of rejected polymer at the membrane's surface.

More complete details of the experiments are given elsewhere.[15]

Results and Discussion

The experimentally determined reflection coefficients are plotted versus MSA flow rate per pore in Figures 2 and 3. Scatter in the data might have been due to fouling of the membrane or the polydispersity of our PBT samples. The former could have occurred from contaminants in the MSA or from PBT aggregation caused by the presence of water. Some experiments, the data from which are not reported here, were prematurely terminated because the membrane hydraulic permeability ($Q/\Delta P$) decreased an unacceptable amount during PBT filtration. For all the data reported here, membrane permeability decreased less than 3% over the course of one experiment (i.e., one value of q). To correct for this small change in hydraulic permeability when computing q from the total flow rate Q ($q = Q/n$), the number of pores (n) was adjusted proportionately to the decrease in permeability. This correction is based on the assumption that the reduction

in permeability occurred because some pores were totally blocked.

The polydispersity of our PBT samples could have contributed to some of the apparent scatter in the data because in one sequence of experiments with one membrane no new PBT was introduced into the high-pressure side of the filtration cell. During the first experiment a greater proportion of the smaller components of PBT might have passed through the membrane, leaving a distribution of PBT more biased toward higher molecular weight in the high-pressure reservoir to begin the next experiment. We noticed a trend of σ slightly increasing at constant q in a sequence of experiments; however, this effect was too small to account for all of the scatter in the data plotted in Figures 2 and 3.

A potential contribution to scatter in the data when comparing the results obtained with different membranes could be the small polydispersity of pore size resulting from overlap of the pores (i.e., tracks etched into each other's domain). The largest porosity, about 6%, occurred with M27, the data from which are plotted as triangular symbols in Figure 2. The larger pores resulting from doublets would tend to channel solutions at a higher flow rate per pore compared to the pore singlets. An analysis of the effects of a bimodal pore size distribution on the measured reflection coefficient, presented in the Appendix, indicates that pore overlap was not an important factor in our experiments.

σ^0, the zero-flow limit of σ, appears to be less than unity for both PBT samples. One might intuitively expect that σ^0 should equal one since $L/2R > 1$ for our experiments. However, as argued by Auvray[11] and discussed more quantitatively below, there is a significant fraction of orientations of a long rod that would allow passage of the rod into the pore in the strong-Brownian limit ($q\eta_s/kT \ll (2R/L)^3$).

The following expression[17] is a good approximation for the reflection coefficient of axisymmetric particles in cylindrical pores when the orientation probability of the particles is controlled by Brownian motion:

$$\sigma^0 \doteq (1-K)^2 \tag{9}$$

where K is the equilibrium partition coefficient of the particles between the pore and bulk solutions. Analytical expressions for K of long rods in circular pores of radius R were derived by Giddings et al.[18] for the case of purely steric interactions:

$$K = 1 - \frac{4}{3\pi\alpha}\left[(1+\alpha^2)E\left(\alpha,\frac{\pi}{2}\right) - (1-\alpha^2)F\left(\alpha,\frac{\pi}{2}\right)\right] \quad \text{for } \alpha < 1$$

$$= 1 - \frac{8}{3\pi} \quad \text{for } \alpha = 1$$

$$= 1 - \frac{4}{3\pi}\left[(1+\alpha^2)E\left(\alpha^{-1},\frac{\pi}{2}\right) - (\alpha^2-1)F\left(\alpha^{-1},\frac{\pi}{2}\right)\right] \quad \text{for } \alpha > 1 \tag{10}$$

where $\alpha = L/2R$ and F and E are elliptical integrals of the first and second kind, respectively. Using these expressions with (9), we constructed one of the plots in Figure 4; the other curve is a more exact calculation for long rods.[15] Auvray[11] predicts $1 - \sigma \sim \alpha^{-2}$ for the Brownian limit of long rods ($\alpha > 1$); eqs 9 and 10 give $1 - \sigma \sim 2K \sim \alpha^{-2}/4$.

The fact that our experimental values of σ as $q \to 0$ are somewhat lower than predicted from Figure 4 might be due to the polydispersity of the PBT samples (see Table III). To correct for the polydispersity, we can average the

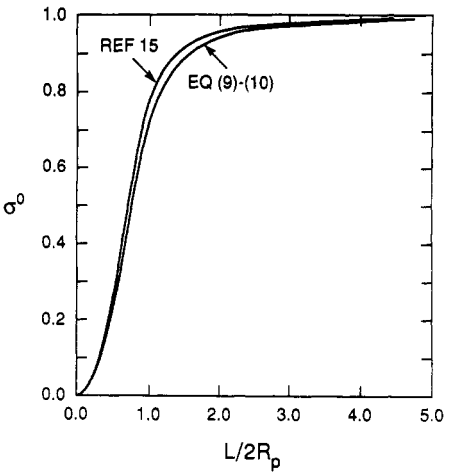

Figure 4. Theoretical predictions for the zero-flow-rate limit of reflection coefficient versus the length (L) of rodlike molecules. R_p is the radius of a circular cylindrical pore.

reflection coefficient according to

$$\langle\sigma^0\rangle = \int_0^\infty \sigma^0 P(L)\, dL \tag{11}$$

where $P(L)$ is the mass fraction of PBT with lengths between L and $L + dL$. The Schulz–Zimm formula for P is chosen[19]

$$P(L) = \frac{y^{h+1}L^h}{\Gamma(h+1)}\exp(-yL) \tag{12a}$$

where Γ is the gamma function and the two parameters y and h are given by

$$\frac{M_w}{M_n} = 1 + \frac{1}{h} \tag{12b}$$

$$L = \frac{h+1}{y}\left[\frac{h+2}{h+1}\right]^{4/9} \tag{12c}$$

where L is the mean length determined from eq 3 and listed in Table I. In addition to PBT polydispersity, pore overlap will also have a small effect on the reflection coefficient.

Theoretical calculations of $\langle\sigma^0\rangle$ were made by using (9)–(12) to account for the distribution of rod lengths for the PBT samples and (A13) to account for pore overlap. Additionally, a correction for the rhomboidal shape of the pores was made by using the radius (R_p) of a circle *inscribed* inside the rhombus, rather than the area-equivalent circle (R), in (10):

$$\alpha = L/2R_p; \quad R_p = 0.825R \tag{13}$$

It can be shown[20,21] that R_p is the appropriate radius for computing the partition coefficient (K) of hard spheres in rhomboidal pores. The results of these calculations are listed in Table III. Taking $M_w/M_n = 2$, as expected for our PBT samples, a closer look (see Appendix A.2) at the factors contributing to $\langle\sigma^0\rangle$ indicates that the polydispersity of the PBT has a greater effect than does the pore overlap even for the membrane with the highest porosity ($\phi = 6.6\%$). A general comparison of Table III with the data in Figures 2 and 3 as $q \to 0$ leads us to conclude that the steric theory for a reflection coefficient based on a rigid-rod model for PBT is appropriate.

Figures 2 and 3 show a flow-rate dependence of σ that is very similar to that for polystyrene filtration.[2-4] The similarity is even more obvious if the PBT data are normalized by σ^0, as shown in Figure 5. To construct this

Table III
Theoretical Predictions of the Zero-Flow-Rate Limit of the Reflection Coefficient ($<\sigma^0>$) for Long Rods in Circular Pores of Radius R_p[a]

polymer	membrane	$L/2R_p$[b]	$<\sigma^0>$[c] for M_w/M_n = 1.0	1.1	2.0
PBT-S	M23	2.32	0.95	0.93	0.77
PBT-S	M24	2.71	0.96	0.94	0.79
PBT-S	M25	3.38	0.97	0.96	0.84
PBT-A	M26	1.55	0.89	0.83	0.63
PBT-A	M27	1.63	0.90	0.84	0.64

[a] The rods are polydisperse with the indicated values of M_w/M_n. [b] R_p is the radius of a circle inscribed in the rhomboidal pore: $R_p = 0.825R$. [c] From (9)–(13) and (A13) of the Appendix.

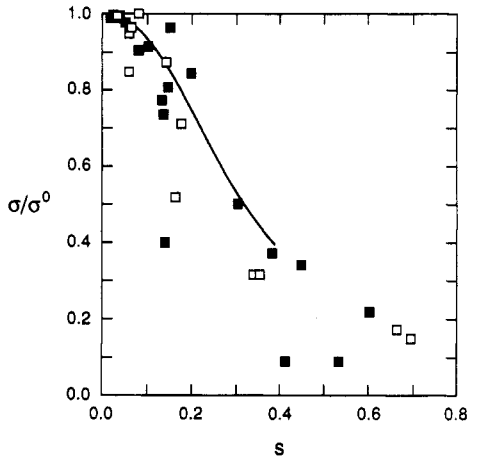

Figure 5. Normalized reflection coefficient of PBT-A (unfilled squares, $\sigma^0 = 0.79$) and PBT-S (filled squares, $\sigma^0 = 0.84$) versus MSA flow rate per pore ($s = q\eta_s/kT$). The curve represents the linear polystyrene data (eq 14).

plot, we used the following values for σ^0: PBT-A, 0.79; PBT-S, 0.84. The solid curve empirically fits the polystyrene data[4] over the range $1 > \sigma > 0.4$ and has the following form:

$$\sigma = [1 + 13.18s^{2.26}]^{-1} \tag{14}$$

When normalized by σ^0, the effects of flow rate on PBT rejection do not appear to depend strongly on the length (molecular weight) of the polymer. Figure 5 suggests that the dynamics of rodlike and flexible chain molecules are similar in the entrance flow of a pore, as proposed by Auvray.[11] Furthermore, the fact that even random-walk chains are statistically elongated, with root-mean-square displacements in the ratio 11:3:1 along three orthogonal axes,[22] may account for this similar behavior.

The pore size distribution arising from overlap of etched tracks could have contributed some ambiguity to the interpretation of the data for σ versus q. This issue is addressed in Appendix A.3 and Figure 6. The larger pores (doublets) cause a smaller overall σ because more flow occurs through them ($q \sim$ (area)^2). However, the calculations of A.3 indicate that even for the membrane having the highest porosity (M27), the doublets reduced σ by a modest amount (<6%) from the value expected if all the pores were singlets. This is because a 6.6% porosity with track-etched membranes results in a rather small standard deviation in pore size.

In summary, we have demonstrated that the filtration of a rodlike polymer at dilute concentrations is flow-rate dependent, with σ being a decreasing function of the flow rate through each pore. An important feature of our experiments is the narrow pore size distribution of the membranes, which allows the data to be interpreted in terms of transport through single pores. The experimental values of the low-flow-rate limit of σ are in reasonable agreement with theoretical predictions based on steric interactions between rigid rods and cylindrical pores. In addition, Figure 5 indicates that the rejection of PBT is quantitatively similar to that of polystyrene in a good solvent, with σ/σ^0 a function of $q\eta_s/kT$, even though the molecular conformations of PBT and polystyrene are greatly different and the viscosity of MSA is 20 times that of chloroform, the solvent used in the polystyrene experiments.

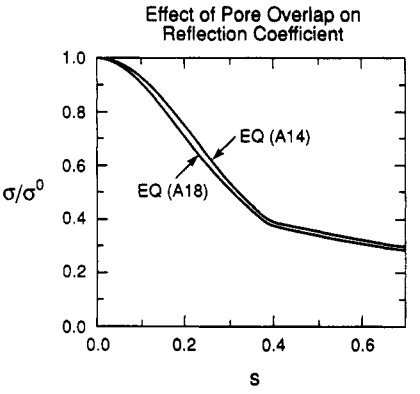

Figure 6. Normalized reflection coefficient for a membrane with porosity $\bar{\phi} = 6.6\%$ and polymer with $M_w/M_n = 2$. Equation A14 assumes all pores are the same size, while (A18) allows for singlets and doublets with the statistical parameters of section A.1.

Acknowledgment. Support for this research was provided by National Science Foundation Grant CBT-8613212. R.P.A. is grateful to the Amoco Foundation for a graduate fellowship. We appreciate the advice and materials provided to us by G. C. Berry and C. Spencer and the discussions with E. D. Glandt on pore overlap in track-etched membranes.

Appendix

A.1. Statistics of Pore Overlap. The track-etch process produced pores of uniform size unless the porosity (pore area fraction) is large enough to cause a significant number of pores to overlap. We consider here the statistical representation of singlets (one distinct pore) and doublets (two pores that overlap) and the consequences of pore overlap on solvent flow and the reflection coefficient.

Let n equal the number of tracks in the area A and R_1 equal the circular, area-equivalent radius of a singlet, with $\phi_0 = n\pi R_1^2/A$. If there were no overlap of pores, then the actual porosity (ϕ) would equal ϕ_0; however, overlap causes $\phi < \phi_0$. If the tracks impinge *randomly* on A and the pores grow by the etching process at a rate independent of the location of their nearest neighbors, then the following expression is exact:

$$\phi = 1 - e^{-\phi_0} \tag{A1}$$

To obtain the number of singlets (n_1), consider the probability that the addition of one more pore results in one more singlet:

$$\frac{dn_1}{dn} = 1 - 4\frac{n_1\pi R_1^2}{A} + O(n_2) \tag{A2}$$

The coefficient 4 appears because it accounts for two tracks that grow (etch) into each other when the centers are separated by $2R_1$; note that the coefficient is also 4 for any regular shape of pore (e.g., rhombus). The term $O(n_2)$ is

neglected; it would represent the target area presented by doublets and is $O(\phi^2)$. Integrating (A2) gives

$$x_1 = n_1/n = 1 - 2\phi_0 \tag{A3}$$

which can also be written as

$$\phi_1 = \frac{n_1 \pi R_1^2}{A} = \phi_0(1 - 2\phi_0) \tag{A4}$$

We note here the error in ref 16, eq 1. Since we are only considering singlets and doublets, we have

$$x_2 = \frac{n_2}{n} = \frac{1 - x_1}{2} = \phi_0 \tag{A5}$$

$$\phi_2 = \phi - \phi_1 = \frac{3}{2}\phi_0^2 \tag{A6}$$

If we define the average radius of a doublet by $n_2\pi R_2^2/A = \phi_2$, then (A5) and (A6) give

$$(R_2/R_1)^2 = 3/2 \tag{A7}$$

That is, the *mean* area of the doublets is 3/2 times the area of a singlet.

The number of tracks (N) is determined from calibrations of irradiation intensity during membrane preparation. The mean pore radius (R) is calculated from the pressure–flow relation measured for the membrane and the following equation:

$$Q = 0.68\frac{n\pi R^4}{8\eta_s l}\Delta P \tag{A8}$$

where l is the membrane thickness and 0.68 is a correction for the rhomboidal geometry of the pores. If all the pores were singlets of area-equivalent radius R_1, then R from (A8) would equal R_1.

With two types of pores, singlets and doublets, we have

$$Q = Q_1 + Q_2 = 0.68\frac{n}{8\eta_s l}[x_1\pi R_1^4 + x_2\pi R_2^4]\Delta P \tag{A9}$$

A minor assumption in (A9) is that the average doublet is a rhombus, so that the coefficient 0.68 can be applied to both singlets and doublets. By combining (A3)–(A9) we have

$$R_1 = R\left[1 - \frac{1}{16}\bar{\phi} + O(\bar{\phi}^2)\right] \tag{A10}$$

where $\bar{\phi} = n\pi R^2/A$. Since $\phi < 0.07$ (see Table II), we have $R_1 \doteq R$ to better than 0.5%. Note also that

$$\phi_0 = \bar{\phi}\left[1 - \frac{1}{8}\bar{\phi}\right] + O(\bar{\phi}^3) \tag{A11}$$

A.2. Effect of Pore Overlap on σ^0. The zero-flow limit of σ for rigid rods can be computed from (9)–(12) and

$$\langle\sigma^0\rangle = Q^{-1}[Q_1\langle\sigma_1^0\rangle + Q_2\langle\sigma_2^0\rangle] \tag{A12}$$

where the brackets denote the average over the distribution of rod lengths according to (11) and the subscript 1 or 2 denotes a singlet or a doublet pore, with R_1 and R_2 given by (A10) and (A7), respectively. Using (A3)–(A10) with (A11) we have

$$\langle\sigma^0\rangle = \langle\sigma_1^0\rangle + 2.25\bar{\phi}[\langle\sigma_2^0\rangle - \langle\sigma_1^0\rangle] + O(\bar{\phi}^2) \tag{A13}$$

The above expression was used to compute the values of $\langle\sigma^0\rangle$ in Table III. The effect of the bimodal pore size distribution is in the second term on the right side of (A13).

In order to evaluate the maximum effect of pore overlap on σ^0 for our experiments, consider membrane M27 (see Table II) with $M_w/M_n = 2$. Using the inscribed circular radius (R_p) to compute α, we have from (9)–(13)

$$\langle\sigma_1^0\rangle = 0.66 \qquad \langle\sigma_2^0\rangle = 0.58$$

The overlap effect in (A13) is given by $2.25\bar{\phi}(\langle\sigma_2^0\rangle - \langle\sigma_1^0\rangle) = -0.01$. Thus, in this worst case the overlap of pores to form doublets reduces $\langle\sigma^0\rangle$ by 2% from the value expected for 100% singlets of radius R_p = 360 Å.

A.3. Effect of Pore Overlap on σ versus Flow Rate. For nonzero flow rates, pore overlap makes experimentally measured reflection coefficients *less* than those calculated assuming all the tracks are separate pores. This effect arises because the overlapping pores channel more of the flow compared to the nonoverlapping pores. Thus, greater extension and orientation will be felt by flexible chains and rigid rods passing through the larger pores. To quantify this effect, assume that eqs 2b and 14 describe the flow-rate dependence of the reflection coefficient for both flexible chains and rigid rods when a membrane has pores of uniform size.

$$\begin{aligned}\sigma/\sigma^0 &= [1 + 13.18s^{2.26}]^{-1} \qquad 0 \le s \le 0.38\\ &= 0.247s^{-1/2} \qquad s > 0.38\end{aligned} \tag{A14}$$

where $s = q\eta_s/kT$ and $q = Q/n$.

Consider now a membrane having singlet and doublet pores. Applying the relations derived in the previous section gives

$$\langle\sigma\rangle = \langle\sigma_1\rangle + 2.25\bar{\phi}[\langle\sigma_2\rangle - \langle\sigma_1\rangle] + O(\bar{\phi}^2) \tag{A15}$$

and

$$s_1 = \frac{Q_1\eta_s}{n_1 kT} = \left(1 - \frac{1}{4}\bar{\phi}\right)s + O(\bar{\phi}^2) \tag{A16}$$

$$s_2 = \frac{Q_2\eta_s}{n_2 kT} = 2.25\left(1 - \frac{1}{4}\bar{\phi}\right)s + O(\bar{\phi}^2) \tag{A17}$$

where s is based on the flow rate per pore if all the pores are singlets of radius R and both $\langle\sigma_1\rangle$ and $\langle\sigma_2\rangle$ are described by eq A14 using s_1 and s_2, respectively.

To investigate the effect of pore overlap on the reflection coefficient at nonzero flow rates, we consider a membrane of porosity = 6.6% (i.e., M27). Assuming a PBT polydispersity of $M_w/M_n = 2$ and using the inscribed area to calculate $\langle\sigma_1^0\rangle$ and $\langle\sigma_2^0\rangle$, we combine (A14)–(A17) to give

$$\begin{aligned}\langle\sigma\rangle/\langle\sigma^0\rangle &= 0.867[1 + 12.70s^{2.26}]^{-1} +\\ &\qquad 0.134[1 + 79.36s^{2.26}]^{-1} \qquad 0 \le s \le 0.17\\ &= 0.867[1 + 12.70s^{2.26}]^{-1} +\\ &\qquad 0.022s^{-1/2} \qquad 0.17 \le s \le 0.39\\ &= 0.238s^{-1/2} \qquad 0.39 \le s\end{aligned} \tag{A18}$$

Figure A1 compares the values of reflection coefficients calculated from (A14) and (A18). In this case pore overlap reduces $\langle\sigma\rangle/\langle\sigma^0\rangle$ by less than 6% from the value calculated by assuming the membrane has pores that are all the same size.

References and Notes

(1) Nguyen, Q. T.; Neel, J. *J. Membr. Sci.* **1983**, *14*, 97.
(2) Long, T. D.; Anderson, J. L. *J. Polym. Sci., Polym. Phys. Ed.* **1983**, *22*, 1261.
(3) Long, T. D.; Anderson, J. L. *J. Polym. Sci., Polym. Phys. Ed.* **1985**, *23*, 191.
(4) Adamski, R. P.; Anderson, J. L. *J. Polym. Sci., Part B: Polym. Phys.* **1987**, *25*, 765.
(5) de Gennes, P.-G. *J. Chem. Phys.* **1978**, *60*, 5030.
(6) Leal, L. G. Studies of Flow-Induced Conformation Changes in Dilute Polymer Solutions. In *Polymer-Flow Interaction*; American Institute of Physics Conference Proceedings, 1985; Rabin, Y., Ed.; No. 137, p 5.

(7) Daoudi, S.; Brochard, F. *Macromolecules* **1978**, *11*, 751.
(8) de Gennes, P.-G. *Scaling Concepts in Polymer Physics*; Cornell University Press: Ithaca, NY, 1979.
(9) Keh, H. J. *J. Chin. Inst. Chem. Eng.* **1985**, *16*, 395.
(10) Odell, J. A.; Keller, A.; Atkins, E. D. T. *Macromolecules* **1985**, *18*, 1443.
(11) Auvray, L. *J. Phys.* **1981**, *42*, 79.
(12) PBT-A and PBT-S were provided by G. C. Berry and C. Spencer of the Chemistry Department, Carnegie Mellon University, Pittsburgh, PA 15213.
(13) Chu, S. G.; Venkatraman, S.; Berry, G. C.; Einaga, Y. *Macromolecules* **1981**, *14*, 939.
(14) Berry, G. C. Properties of Solutions of Rodlike Chains from Dilute Solutions to the Nematic State. *Proceedings of the Materials Research Society*, Boston, Nov 1988.
(15) Adamski, R. P. Ph.D. Thesis, Carnegie Mellon University, Pittsburgh, PA, 1987.
(16) Quinn, J. A.; Anderson, J. L.; Ho, W. S.; Petzny, W. J. *Biophys. J.* **1972**, *12*, 990.
(17) Anderson, J. L. *J. Theor. Biol.* **1981**, *90*, 405.
(18) Giddings, J. C.; Kucera, E.; Russel, C. P.; Myers, M. N. *J. Phys. Chem.* **1968**, *72*, 4397.
(19) Berry, G. C. Polymers: Molecular Weight and its Distribution. In *Encyclopedia of Materials Science and Engineering*; Bever, M. D., Ed.; Pergamon Press: New York, 1987; p 3759.
(20) Malone, D. M.; Anderson, J. L. *Chem. Eng. Sci.* **1978**, *33*, 1429.
(21) Glandt, E. D. *J. Membr. Sci.* **1981**, *8*, 331.
(22) Rudnick, J.; Gaspari, G. *Science* **1987**, *237*, 384.

Registry No. PBT, 69794-31-6; MSA, 75-75-2.